Think Modular: A Simple Apoferritin-Based Platform for the Multifaceted Detection of Pancreatic Cancer

Mintai P. Hwang,[†] Jong-Wook Lee,[†] Kyung Eun Lee,[‡] and Kwan Hyi Lee[†,*]

[†]Center for Biomaterials, Biomedical Research Institute, Korea Institute of Science and Technology (KIST), 5 Hwarangno 14-gil, Seongbuk-gu, Seoul 136-791, Republic of Korea and [‡]Advanced Analysis Center, Korea Institute of Science and Technology (KIST), 5 Hwarangno 14-gil, Seongbuk-gu, Seoul 136-791, Republic of Korea

ABSTRACT The generation of nanosized probes often requires time-intensive and application-specific optimization processes that involve conjugating a nanoconstruct to a targeting moiety. Herein, we genetically modify apoferritin and generate a universal interface system composed of protein G and 6×His-tag. The resulting construct, conferred with modularity and high targeting efficiency, is applied toward two distinct applications in the detection of a pancreatic cancer biomarker and used to demonstrate its potential in the facile exchange of nanoprobe components.

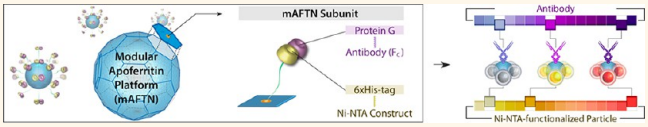

KEYWORDS: apoferritin · modular · quantum dot · gold nanoparticle · pancreatic cancer

Recent advances spanning different fields of research continue to reveal a variety of nanosized substances in the commercial, industrial, and governmental sectors.[1,2] The emergence of the proteomics field, for example, has yielded a number of biomarkers for the early detection of cancer, while that of green science and technology has generated an increased awareness for environmental toxins such as heavy metals and biological agents.[3−6] Probes, in the broadest sense of the term, are commonly employed to meet the growing demand for the detection and quantification of such target analytes.

Nanosized probes are particularly attractive for a number of reasons that include, but are not limited to, the following: (1) a high surface-area-to-volume ratio for the maximization of target interaction,(2) small physical size for the minimization of size-induced steric hindrance, and(3) the capacity to take advantage of unique physical, chemical, and optical properties that naturally materialize at the nanoscale. From simple organic substances such as proteins and liposomes, synthetics such as dendrimers, to inorganic materials such as quantum dots or gold nanoparticles, a wide spectrum of nanoconstructs form the foundational for subsequent implementation into a functional probe. For instance, a dendrimer-based system uses aptamers (ligand-binding nucleic acids) for the detection of *Botulinum* neurotoxin.[7] In another example, gold nanoparticles are surface-conjugated with yeast iso-1-cytochrome C *via* a thiol group and used to detect changes in pH.[8] In a different study, CdSe quantum dots are labeled with metalloprotein for the detection of maltose.[9]

Prima facie, these various probes are a collection of random parts. A closer look, however, reveals an organized assembly of components, the specifics of which are determined by the application. In other words, each of the biosensor probes is composed of a basic construct (*i.e.*, dendrimers, gold nanoparticles, protein cages, *etc.*), an adaptor unit (*i.e.*, chemical unit, enzymes, *etc.*), and a targeting moiety (antibody, peptide, aptamer, *etc.*). It is important to note that the different probes are developed out of a context-driven template in which the application determines the type of components needed during the assembly of the nanoconstruct probe. Consequently, any application of the nanoconstruct probe is often preceded by time-consuming and often challenging heuristic optimization methods. In addition, it is important to note that many nanoconstruct probes are generated *via* a nonspecific chemical reaction between the different

* Address correspondence to kwanhyi@kist.re.kr.

Received for review July 8, 2013 and accepted August 27, 2013.

Published online August 29, 2013
10.1021/nn403465a

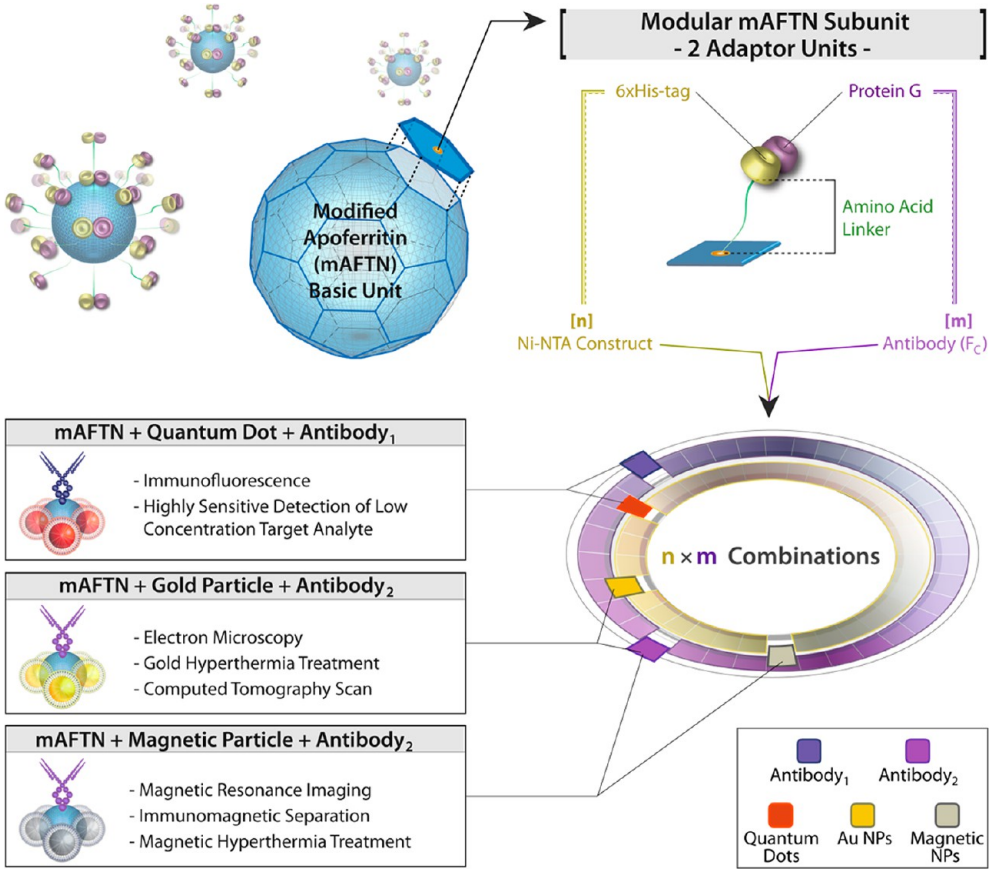

Scheme 1. Apoferritin-based modular nanoconstruct. Each of the 24 heavy chain apoferritin subunits is genetically modified to express two adaptor units: 6×His-tag and protein G. The resulting modified apoferritin (mAFTN) basic unit can be conjugated with a construct surface-functionalized with Ni-NTA *via* interaction with its 6×His-tag adaptor unit, and with an antibody *via* interaction with its protein G adaptor unit. A wide range of different nanoconstruct probes can be produced from the modular mAFTN basic unit by combining one of the 'n' types of constructs surface-functionalized with Ni-NTA derivatives with one of the 'm' types of antibodies commercially available. Three examples have been listed to demonstrate the potential to use mAFTN as a modular nanoconstruct.

components, such as the use of carboiimide-based NHS/EDC chemistry. While such approaches are well-established, more importantly, they deprive the nanoconstruct probe of directionality. For instance, the lack of proper spatial presentation of the targeting moiety not only results in a decreased targeting efficiency and thus increased expense, but also increases the chance of nonspecific interactions between the nanoconstruct probes and therefore that of the probability of aggregation. In this context, a universal interface system capable of providing a means to overcome application-specific demands is invaluable. Furthermore, the ability to spatially orient targeting moieties to ensure maximum detection functionality is a necessary and practical setup. Put simply, a modular nanoconstruct conferred with directionality of its targeting moiety is highly desirable for the facile construction of a wide range of probes.

Herein, we propose to transform human apoferritin[10] (AFTN) into a modular construct for the facile exchange of different sets of components (Scheme 1). Heavy chain AFTN subunits are genetically modified to express protein G and 6×His-tag, which act in tandem to confer a universal interface system to the self-assembled nanoconstruct. Specifically, any antibody and Ni-NTA-functionalized nanoparticle can be bound *via* protein G and 6×His-tag,[11,12] respectively, to form unique probes; the modularity and high targeting efficiency of the platform is demonstrated *via* two separate instances in the detection of Claudin-4, an integral membrane pancreatic cancer biomarker that is highly expressed in the tight junctions of pancreatic cancer cells.[13]

RESULTS AND DISCUSSION

AFTN, a highly conserved protein for the storage and transportation of iron, is composed of 24 subunits which undergo self-assembly to form a 4-helical bundle in the form of a hollow spherical shell.[10] Generally, the 24 subunits are composed of two types, H (heavy) and L (light), and assemble in different ratios to form a variety of isoferritins.[14,15] By genetically modifying the H subunit to express two types of universal adaptor units (Figure 1A), and by taking advantage of the natural self-assembly of AFTN into spherical shells, we generate a modular unit of H subunit-based apoferritin (mAFTN). Specifically, each subunit is induced to express protein G (a cell-surface protein on

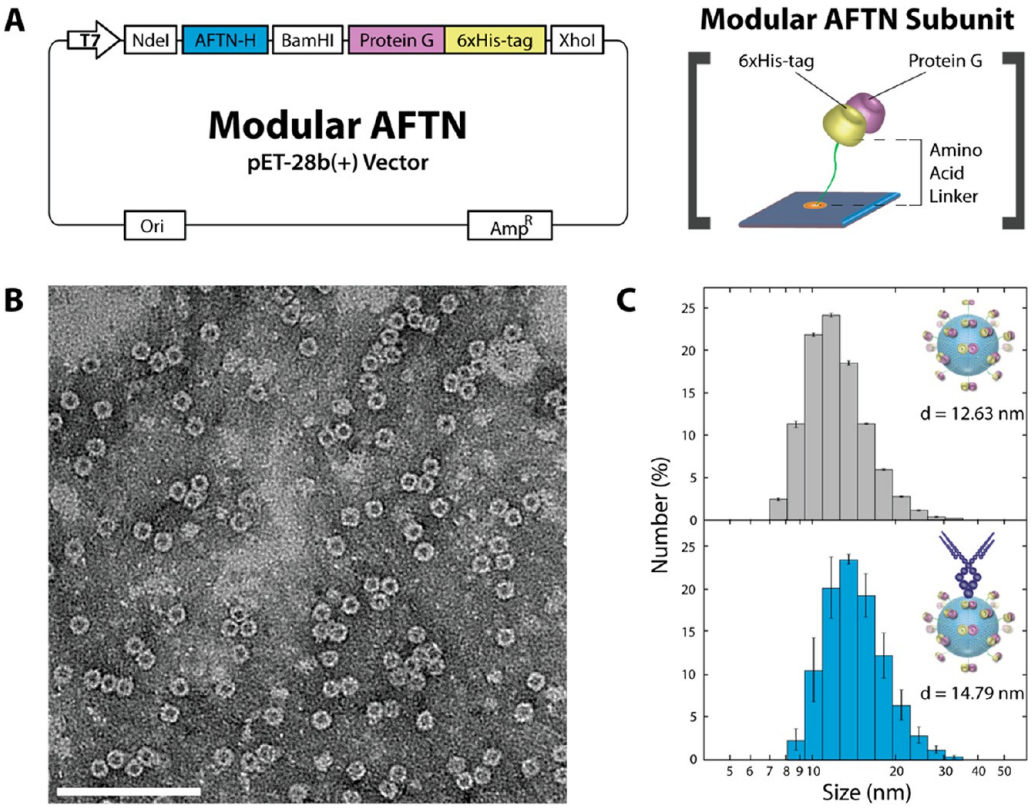

Figure 1. Engineering apoferritin to use as a modular construct. (A) A modular AFTN construct (mAFTN) is engineered by genetically modifying heavy chain apoferritin (AFTN-H) to generate a fusion protein construct with protein G and 6×His-tag. Both adaptor units are expressed on the extraluminal surface of each mAFTN subunit. (B) TEM image of hollow spherical shells indicate proper self-assembly of mAFTN subunits (scale bar = 100 nm). (C) Size distribution of intermediate mAFTN−aCLDN4 nanoconstructs as assessed *via* DLS measurements (n = 3).

streptococcal bacteria) and 6×His-tag, which interact with the Fc region of antibodies and nickel-nitriolotriacetic acid (Ni-NTA), respectively, in a well-documented manner.[11,12,16−19] Individually, the charged/polar interaction between protein G and the Fc region of an antibody has an equilibrium constant of approximately $1.13 \times 10^8\ M^{-1}$, while the coordination bond between a 6×His-tag and Ni-NTA has a dissociation constant of approximately 1×10^{-13}.[20,21] Here, the use of protein G confers directionality to the targeting moiety in that protein G binds to the Fc region of an antibody, thereby orienting the antibody in an outward direction and thus rendering the Fab region sterically accessible. Furthermore, the use of 6×His-tag enables the conjugation of any additional construct to mAFTN provided its surface-modification with Ni-NTA. In essence, given the wide availability of commercial antibodies and the ease with which components can be surface-modified with Ni-NTA derivatives, the introduction of two universal adaptor units, 6×His-tag and protein G, provides the flexibility to engineer a number of different types of antibody/Ni-NTA-based nanoconstruct probes from a single mAFTN unit. In this study, we demonstrate the feasibility of mAFTN as a modular construct through two distinct applications in the detection of Claudin-4 (CLDN4), a pancreatic cancer biomarker. For both applications, a bacterial expression system is used to synthesize mAFTN with the extraluminal surface expression of 6×His-tag and protein G. Gene sequencing indicates proper synthesis of mAFTN (Supporting Information Figure S1), and the successfully engineered mAFTN exhibits a spherical morphology with an average outer diameter of 12.63 nm as assessed *via* transmission electron microscopy (TEM) and dynamic light scattering (DLS) measurements (Figure 1, panels B and C, respectively). For the purpose of this study, anti-CLDN4 antibodies (aCLDN4) are then added in equal molar concentration to mAFTN, followed by purification *via* microfiltration to ensure removal of unconjugated aCLDN4. Purified mAFTN/aCLDN4 intermediate constructs have an average hydrodynamic diameter of 14.79 nm and retain a size distribution profile similar to that of mAFTN as assessed by DLS (Figure 1C). It is important to note the potential modularity of the mAFTN nanoconstruct in which aCLDN4 can be replaced with any other antibody by utilizing the protein G adaptor unit. Furthermore, it is worth mentioning that the number of antibodies bound per mAFTN could be modified for an entirely different set of applications, in which modularity is conferred through the ability to easily change the number of conjugated constructs (*e.g.*, an

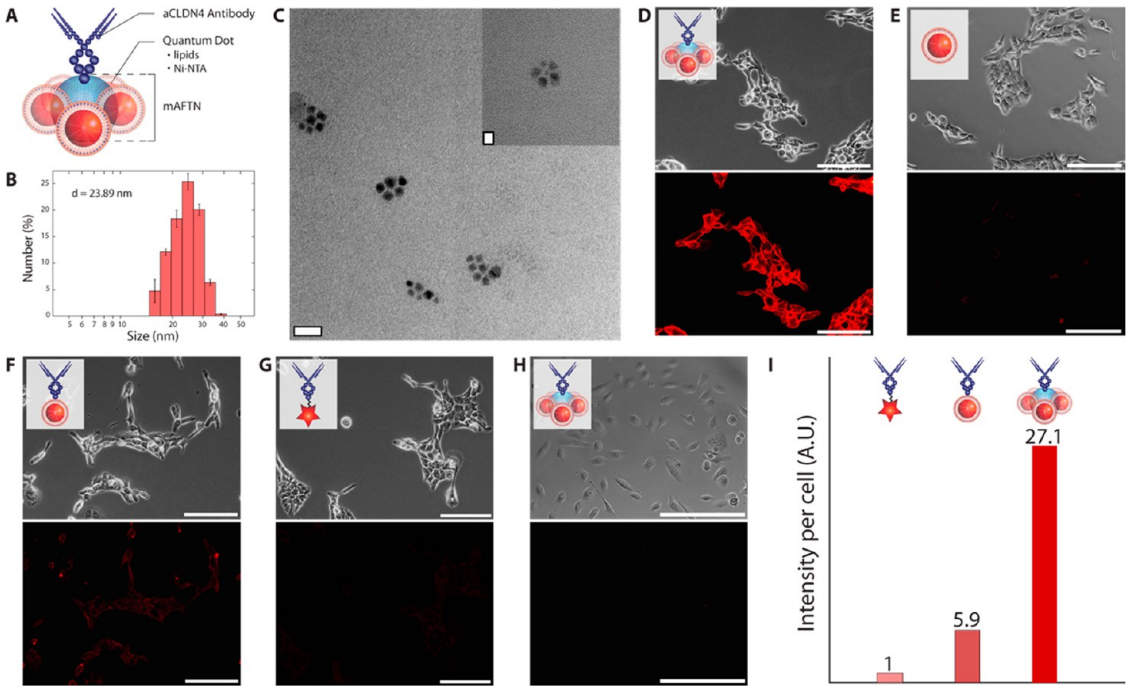

Figure 2. Fabrication of mAFTN-QD nanoconstruct probes for the supersensitive detection of CLDN4 *via* fluorescence. (A) Schematic representation of multiple water-solubilized and Ni-NTA-functionalized CdSe(ZnS) QDs bound to a mAFTN−aCLDN4 complex. (B) mAFTN-QD nanoconstruct probes are approximately 23.89 nm in diameter (n = 3). (C) TEM image of mAFTN-QD nanoconstruct probes (main image scale bar = 20 nm; inset scale bar = 5 nm). (D) Phase contrast and fluorescence images of targeted CLDN4 on Capan-1 cells are taken after treatment with mAFTN-Ab-QD, (E) QD only, (F) aCLDN4-QD, and (G) aCLDN4-564. (H) Phase contrast and fluorescent images of HPDE cells are taken after incubation with mAFTN-Ab-QD. Scale bars for both phase contrast and fluorescent images represent 200 μm. (I) Relative intensity measurements per cell demonstrate an approximately 27-fold increase in fluorescence detection sensitivity for mAFTN-QD nanoconstruct probes over conventional fluorophores.

efficient capture system in which mAFTN is conjugated with multiple antibodies to generate a type of "nanosponge").

In the first application, we apply CdSe(ZnS) quantum dots (QDs) to the mAFTN/aCLDN4 constructs to generate a mAFTN-QD nanoconstruct probe capable of the highly sensitive detection of CLDN4 (Figure 2A). QDs, an inorganic material with excellent optical properties compared to those of conventional organic fluorophores,[22,23] are conjugated in excess to a single unit of mAFTN, thereby providing a means to increase the signal output. The natural affinity of 6×His-tag on mAFTN for Ni-NTA on QDs is used in the conjugation of QDs to mAFTN. Given that the CdSe(ZnS) QDs are prepared in organic solvents, they are first water-solubilized using a combination of lipids as previously described[24] and functionalized with a minute amount of Ni-NTA. Water-solubilized and Ni-NTA-functionalized QDs exhibit minimal aggregation (Supporting Information Figure S2A), have an average diameter of 10.32 nm (Supporting Information Figure S2B), and retain an excellent quantum yield of approximately 90% (Supporting Information Figure S2C). The increase in hydrodynamic diameter of the processed QDs may be larger than expected when compared to unprocessed QDs due to the presence of lipids around the processed QDs, which act to increase the microviscosity around the NPs and in effect, the apparent diameter. The successful conjugation of multiple QDs onto mAFTN is verified *via* an increase in the mean size of the nanoconstructs (Figure 2B) and further corroborated through TEM images (Figure 2C) of the mAFTN-QD nanoconstruct probes. Furthermore, given that the addition of excess imidazole liberates Ni-NTA-functionalized QDs from protein G,[25] the conjugation of QDs to mAFTN is based on the interaction between Ni-NTA and 6×His-tag rather than other nonspecific interactions. Finally, the targeting capacity of the mAFTN-QD nanoconstruct probes for CLDN4 is demonstrated *in vitro* by adding them to a pancreatic cancer cell line (Capan-1), which overexpresses CLDN4 (Figure 2D).[26] To exclude the possibility of functionalized QDs binding to Capan-1 cells *via* the interaction between Ni moieties on the QD with histidine amino acids on native Capan-1 proteins, only QDs are administered to the cells (Figure 2E). In-depth analyses by other groups with regards to the binding kinetics of histidine to Ni-NTA provide further evidence that Ni-NTA preferentially forms significantly more stable bonds with 6×His-tags than with single or even double histidine residues.[27] Also, to determine an estimate of number of QDs per mAFTN unit, an additional control group (Figure 2F) in which a single QD is conjugated to a single aCLDN4 *via* protein G is used as previously described.[28] Furthermore, a commercially available aCLDN4 antibody

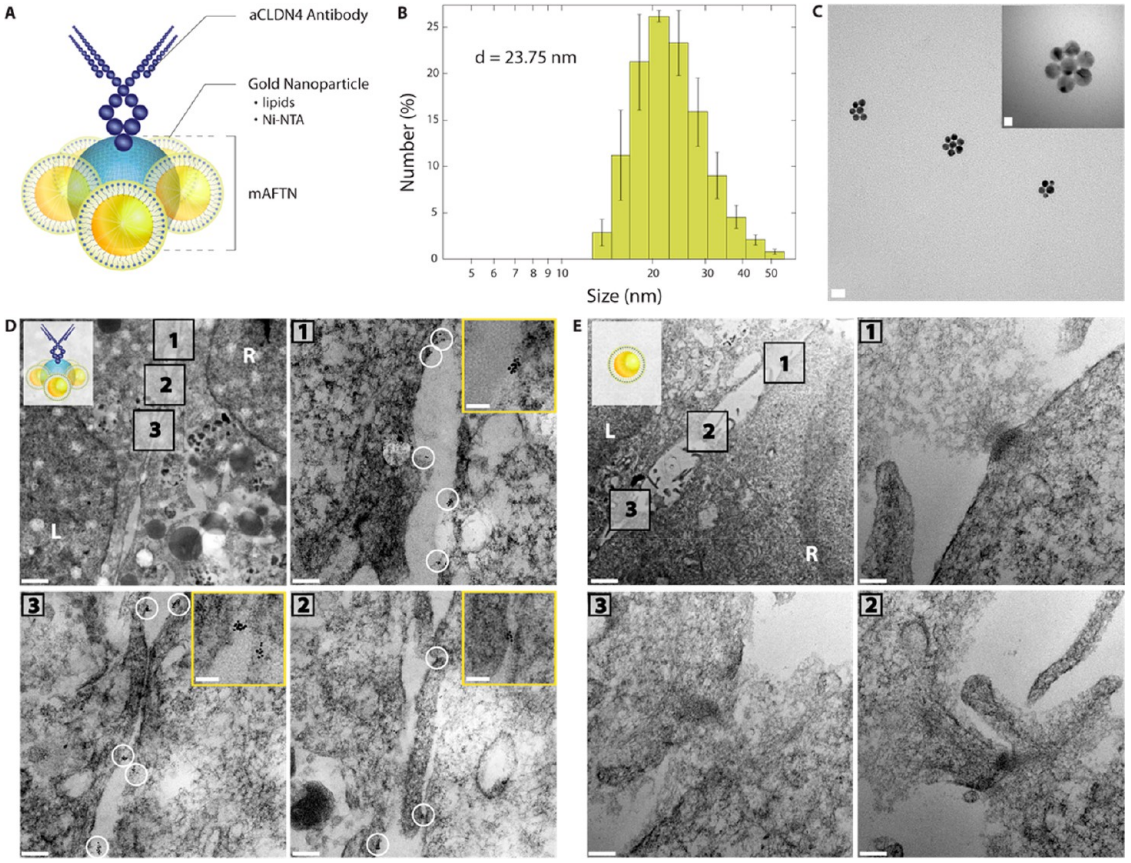

Figure 3. Fabrication of mAFTN-Au nanoconstruct probes for a detailed examination of CLDN4 distribution *via* electron microscopy. (A) Schematic representation of multiple water-solubilized and Ni-NTA-functionalized Au nanoparticles bound to a mAFTN−aCLDN4 complex. (B) mAFTN-Au nanoconstruct probes are approximately 23.75 nm in diameter as assessed *via* DLS measurements ($n = 3$). (C) TEM image of mAFTN-Au nanoconstruct probes (main image scale bar = 20 nm; inset scale bar = 5 nm). (D) TEM images of the intercellular region of Capan-1 cells are taken after treatment with mAFTN-Au (white circles indicate clusters of Au nanoparticles) and (E) Au only. Scale bars for the top left images represent 1 μm and the scale bars for images 1, 2, and 3 represent 100 nm. Scale bars for the insets for images 1, 2, and 3 in panel D represent 50 nm.

conjugated with a fluorophore (Alexa 564) is used as an internal control (Figure 2H). Finally, to verify specificity of the mAFTN-QD nanoconstruct probes for CLDN4, the probes are administered to Human Pancreatic Ductal Epithelial (HPDE) cells, which do not express any CLDN4 (Figure 2H). Through a comparative analysis in signal intensity among the different groups, we demonstrate an approximately 27-fold increase in the fluorescence detection sensitivity over conventional organic fluorophores and a 6-fold increase over single QDs (Figure 2I). Put simply, the mAFTN-QD nanoconstruct probes exhibit an approximately 4.5-fold increase in intensity over single QDs. In other words, assuming a linear relationship between the number of QDs and the resulting signal intensity, we estimate that each mAFTN unit is therefore capable of harboring between 4 and 5 QDs. However, when taking into account the similar size and spherical shape of QDs (average hydrodynamic diameter = 10.32 nm) and mAFTN units (average hydrodynamic diameter = 12.63 nm), we should expect to see approximately 6 QDs bound per mAFTN unit. Furthermore, TEM images indicate approximately 5 to 6 QDs per mAFTN unit (Figure 2C). This slight discrepancy could be attributed to the close distance between the multiple QDs conjugated to mAFTN, which could act to quench the fluorescence signal emitted by the mAFTN-QD nanoconstruct probes, thereby underestimating the number of QDs per mAFTN unit. In essence, given the dichotomy between current technological limitations and the emerging demand for a sensor that can overcome issues of sensitivity at low analyte concentrations that often beset fluorescent-molecule-based probes, the highly sensitive mAFTN-QD nanoconstruct probes are a promising alternative. Furthermore, the quantifiable optical properties of QDs[29] used in the constructs can be utilized to determine absolute numbers of biomarkers,[24] and could provide additional insight.

Such fluorescence imaging is excellent in its ease of use and capacity to provide information on the presence of a biomarker on a widespread cellular level. To provide further information, such as the spatial distribution of biomarker at the subcellular level, electron microscopy (EM) is commonly used during which gold nanoparticle (AuNP) conjugates are extensively employed for their high electron density. In the second application, we fabricate mAFTN-AuNP nanoconstruct

probes by applying functionalized AuNPs to the same basic mAFTN/aCLDN4 constructs used in the first application, and subsequently use them to examine the spatial distribution of CLDN4 on Capan-1 *via* TEM. The AuNPs used in this application are synthesized and subsequently surface-modified with readily available derivatives of Ni-NTA (Supporting Information Figure S3A). Furthermore, the functionalized AuNPs, which yield an average hydrodynamic diameter of 8.7 nm (Supporting Information Figure S3B), exhibit maximum absorbance at a gold-specific wavelength of approximately 520 nm (Supporting Information Figure S3C), indicating that the functionalization process has no effect on the optical properties of gold. Multiple surface-modified AuNPs are then bound to intermediate mAFTN−aCLDN4 constructs through the 6×His-tag adaptor unit (Figure 3A) to yield mAFTN-AuNP nanoconstruct probes with an average diameter of 23.75 nm (Figure 3B). It should be noted that the size distribution profile is retained, indicative of a relatively homogeneous population of hybrid nanoconstructs with a similar number of AuNPs per mAFTN unit. The conjugation of multiple AuNPs onto mAFTN is further confirmed *via* TEM (Figure 3C). To determine the targeting capacity of the mAFTN-AuNP nanoconstruct probes, they are applied to Capan-1 and imaged *via* TEM to obtain subcellular level information on the spatial distribution of CLDN4, a component of cellular tight junctions (Figure 3D). TEM images of Capan-1 targeted with the nanoconstruct probes indicate a spatial preference of CLDN4 toward the intercellular region of Capan-1. On the other hand, the absence of functionalized AuNPs in the control TEM images demonstrates minimal nonspecific binding of AuNPs to the cells *via* interaction between the Ni-NTA moieties on AuNPs and the single histidine residues on the cells, thereby demonstrating a specific targeting capacity of the mAFTN-AuNP nanoconstruct probes for CLDN4 (Figure 3E). It is worth noting that the clusters of AuNPs observed in Figure 3C opens the possibility for a more efficient means of hyperthermal anticancer treatment over that of single AuNPs. Further opportunities lie within *in vivo* applications, given the small size of the hybrid nanoconstruct probe and the biocompatibility of FTN (data not shown) and AuNPs. It should, however, be noted that a potential limitation in the current setup for prospective *in vivo* applications lies in the use of Ni-NTA and its potential toxicity. In addition, the interaction between Ni-NTA and histidine has been shown to be dependent on extrinsic factors such as pH and ionic strength. Consequently, the generation of a covalent bond between histidine and Ni-NTA, followed by quenching of Ni^{2+} ions,[30] could be an alternative method that is both biocompatible and independent of such extrinsic factors. Furthermore, potential limitations due to the use of Ni-NTA can effectively be circumvented by switching the type of universal adaptor unit to other common interactions (*e.g.*, biotin and streptavidin).

CONCLUSIONS

In conclusion, we have presented a modular system based on human heavy chain apoferritin. The potential of modularity of the nanoconstruct is provided on two fronts: (1) the directional binding of any antibody *via* the interaction between its Fc region and the adaptor unit protein G, and (2) the binding of any nanoparticle *via* the interaction between Ni-NTA moieties on its surface and the adaptor unit 6×His-tag. The resulting mAFTN-based nanoconstruct probe is limited only by the number of commercially available antibody with regards to its targeting specificity. Along the same lines, most nanoparticles can easily be surface-modified with Ni-NTA derivatives, effectively presenting a means to append any nanoparticle to the mAFTN-based nanoconstruct probe. Herein, we have demonstrated two distinct applications as a proof-of-concept of the modularity of the system. It is worth noting that the current modular system can be further expanded when considering other potential uses of apoferritin. For instance, a pH-dependent assembly and disassembly mechanism[31] could be used to generate a unit hybrid nanoconstruct consisting of multiple types of nanoparticles. Additionally, different functionalities of H and L subunits and their expression correlation with tissue type and the physiological state of cells[32,33] could be taken into account to form different isoferritin combinations for added functionality. Furthermore, the hollow core of apoferritin, which has been utilized to encapsulate various materials for a number of different applications,[34−36] could be loaded with therapeutic drugs for site-selective release and treatment of various cancers. Finally, when considering that the type of universal adaptor unit can be switched *via* genetic manipulation to utilize other common interactions, the possibilities are further expanded. In essence, an AFTN-based universal interface system composed of 6×His-tag and protein G adaptor units confers simplicity and flexibility to the resulting hybrid nanoconstruct probe and, with it, has the potential to impact various fields.

METHODS

Genetic Modification of Apoferritin. The gene for human heavy-chain apoferritin was purchased from Origene (FTH1: NM_002032) and inserted into a T7-based pET-28b(+) vector flanked by restriction enzymes NdeI and BamHI. The gene for protein G was provided by GeneScript in a pUC57 plasmid cloning vector, and excised for insertion into the pET-28b(+) vector. The gene sequences for protein G and 6×His-tag were

inserted near the C-terminus for their extraluminal orientation. The vectors for the expression of mAFTN were amplified by heat-shock treatment into DH5α (NEB #C2987H), and expressed and self-assembled in BL21 bacterial cells (Koramdeolab). Finally, the bacterial cells were lysed *via* tip sonication and mAFTN was purified using Ni-NTA His-Bind Resin (Qiagen #70666) and a Ni-NTA buffer kit (Novagen #70899-3). mAFTN was sent to Cosmogenetech for gene sequence analysis.

Water-Solubilization and Ni-NTA Functionalization of Quantum Dots. 1-Myristoyl-2-hydroxy-*sn*-glycero-3-phosphocholine (MHPC; Avanti Polar Lipids, Inc. #855575), 1,2-distearoyl-*sn*-glycero-3-phosphoethanolamine-*N*-(methoxy polyethylene glycol)-2000 (DPPE-PEG2000; Avanti Polar Lipids, Inc. #880120), and 1,2-dioleoyl-*sn*-glycero-3-*N*-(5-amino-1-carboxypentyl) iminodiacetic acid succinyl nickel salt (Ni-NTA; Avanti Polar Lipids, Inc. #790404) were added in a 80%, 15%, 5% mol ratio to a chloroform solution of quantum dots (QDs; QD Solution Nanodot HE-series 100−620 nm). The resulting solution was added dropwise to 2 mL of distilled water (DI water), briefly sonicated for 1 min, and continually heated for 1 h at 90 °C to evaporate excess chloroform and facilitate the exchange of solvent into DI water. The subsequent water-solubilized QD solution (surface modified with MHPC, PEG, and Ni-NTA) was sonicated for 30 min to ensure single particle suspension and spun at 14000*g* for 10 min. The supernatant was collected and filtered through a 0.2 μm syringe filter for further removal of any aggregates. To measure the quantum yield of the water-solubilized and functionalized QDs, a Protoflex Quantum Efficiency Measurement System (QE-1100) was used to measure the number of photons absorbed and those emitted as photoluminescence upon excitation at 365 nm. After a baseline was set using a reference sample (DPBS), the ratio of photons emitted as photoluminescence to those absorbed by the QDs was calculated to find the quantum yield.

Synthesis of Gold Nanoparticles and Ni-NTA Functionalization. Gold nanoparticles (AuNPs) were synthesized by adding 30 wt % $HAuCl_4$ in HCl solution (Sigma-Aldrich #334049) to oleylamine (Sigma-Aldrich #O7805) at 60 °C. The resulting mixture was magnetically stirred for 15 min, then stirred at 120 °C for 30 min, and finally stirred at 210 °C for 1 h. The mixture was slowly cooled and immersed in ethanol for subsequent washing steps. Each wash cycle consisted of centrifugation at 5000 rpm for 10 min, followed by removal of supernatant and resuspension in ethanol. After three washing cycles, the samples were left to dry for 3 h and ultimately resuspended in hexane. The synthesized AuNPs were then water-solubilized and functionalized with Ni-NTA in the same manner as QDs.

Fabrication and Characterization of Various Nanoconstruct Probes. mAFTN, purified and dialyzed into PBS, was incubated with an equivalent molar amount of mouse anti-human-CLDN4 monoclonal antibody (Invitrogen #329400) at room temperature for 1 h to yield intermediate mAFTN/aCLDN4 nanoconstructs. To ensure removal of unconjugated CLDN4 monoclonal antibody, the reaction solution was purified *via* centrifugation through a Nanosep microfiltration device at 14 000*g* for 3 min (Pall Corporation #OD300C34). Purified intermediate mAFTN/aCLDN4 constructs were subsequently analyzed with dynamic light scattering (Malvern Zeta-sizer) to generate a size distribution profile. Water-solubilized and Ni-NTA-functionalized QDs or Au nanoparticles were then added to mAFTN/aCLDN4 at a 10-fold molar excess amount and incubated at room temperature for 2 h. Size distribution profiles were obtained for both resulting nanoconstruct probes, and TEM images were taken after sample preparation (FEI G2 F20 Tecnai).

Cell Culture and Maintenance. Capan-1 cells were purchased from Korean Cell Line Bank (KCLB #30079) at passage 39 and maintained in Iscove's Modified Dulbecco's Medium (IMDM; Invitrogen #12440-061) supplemented with 20% FBS and 1% antibiotic-antimycotic (Invitrogen #15240-062). Human Pancreatic Ductal Epithelial (HPDE) cells were a generous gift from Dr. Jong Kyun Lee of the Samsung Medical Center and maintained in Keratinocyte-SFM supplemented with human recombinant Epidermal Growth Factor (rEGF), Bovine Pituitary Extract (BPE), and 1% antibiotic-antimycotic (Invitrogen #15240-062). For immunofluorescence experiments, cells were seeded onto 24-well plates and incubated for 3 days before subsequent fixation with 3.7% formaldehyde. For TEM imaging experiments, cells were seeded onto Cell Desk LF1 coverslips (Sumitomo Bakelite Co., Ltd. #MS-92132) and incubated for 3 days before subsequent fixation with 3.7% formaldehyde.

Fluorescence Imaging of CLDN-4. Capan-1 and HPDE cells were incubated for 3 days in 24 well plates before fixation with 3.7% formaldehyde at 4 °C for 1 h. Fixed cells were then washed with DPBS (Mg^{2+}, Ca^{2+} free) three times and incubated with blocking buffer #1 (50 mM NH_4Cl) for 15 min at room temperature. Upon a washing step with DPBS twice, the cells were then incubated with 2.13 nM of experimental (mAFTN conjugated with aCLDN4 antibody and QDs) and control groups diluted in blocking buffer #2 (20 mM imidazole, 200 mM NaCl, 0.1% BSA, 0.05% Tween 20) for 2 h at room temperature. The appropriate molar amount of experimental and control groups was optimized to fully saturate all CLDN-4 receptors on the Capan-1 cells (data not shown). Finally, the cells were washed with DPBS twice and imaged under phase contrast (10 ms exposure time) and fluorescence settings (200 ms exposure time; excitation filter, BP 350/50; emission filter, BP 605/52) using a Leica DMI6000B AFC microscope.

Transmission Electron Microscopy Imaging of CLDN-4. Capan-1 cells were incubated for 3 days on Cell Desk LF1 coverslips (Sumitomo Bakelite Co., Ltd. #MS-92132) before fixation with 3.7% formaldehyde at 4 °C for 1 h. Fixed cells were treated in the same manner as done for fluorescence imaging, incubated with experimental (mAFTN conjugated with aCLDN4 antibody and Au nanoparticles) and control (Ni-NTA functionalized Au nanoparticles) groups, washed with DPBS twice to wash away any unbound constructs, and stored in 4% glutaraldehyde prior to TEM sample preparation. For TEM sample preparation, the cells were washed with 0.1 M cacodylate buffer, post-fixed in 1% OsO_4 for 1 h at 4 °C, and stained en bloc with 2% uranyl acetate overnight. The sample cells were then serially dehydrated in ethanol (15 min each in 50, 70, 80, 90, 95 and 100%) and embedded in Spur's resin. After polymerization for 24 h at 60 °C, the embedded specimens were sectioned at the thickness of 50 nm on Formvar coated slot grids, stained with 2% uranyl acetate in 50% methanol followed by lead citrate, and observed *via* TEM (Tecnai-G2, FEI, The Nethelands).

Conflict of Interest: The authors declare no competing financial interest.

Acknowledgment. The authors would like to gratefully acknowledge the financial support provided by the Korea Institute of Science and Technology (KIST Institutional Project #2E23720 and K-GRL #2Z03720). We would also like to thank Dr. Jong Kyun Lee of Samsung Medical Center for kindly donating HPDE cells for use as a control.

Supporting Information Available: A figure of gene sequence analysis for genetically modified apoferritin (Figure S1); a figure of the water-solubilization and functionalization of quantum dots, and their characterization (Figure S2); a figure of the water-solubilization and functionalization of gold nanoparticles, and their characterization (Figure S3). This material is available free of charge *via* the Internet at http://pubs.acs.org.

REFERENCES AND NOTES

1. Adler-Abramovich, L.; Kol, N.; Yanai, I.; Barlam, D.; Shneck, R. Z.; Gazit, E.; Rousso, I. Self-Assembled Organic Nanostructures with Metallic-Like Stiffness. *Angew. Chem., Int. Ed.* **2010**, *49*, 9939–9942.
2. Saleh, N.; Phenrat, T.; Sirk, K.; Dufour, B.; Ok, J.; Sarbu, T.; Matyiaszewski, K.; Tilton, R. D.; Lowry, G. V. Adsorbed Triblock Copolymers Deliver Reactive Iron Nanoparticles to the Oil/Water Interface. *Nano Lett.* **2005**, *5*, 2489–2494.
3. Honda, K.; Hayashida, Y.; Umaki, T.; Okusaka, T.; Kosuge, T.; Kikuchi, S.; Endo, M.; Tsuchida, A.; Aoki, T.; Itoi, T.; *et al.* Possible Detection of Pancreatic Cancer by Plasma Protein Profiling. *Cancer Res.* **2005**, *65*, 10613–10622.
4. Patterson, S. D.; Aebersold, R. H. Proteomics: The First Decade and Beyond. *Nat. Genet.* **2003**, *33*, 311–323.
5. Yee, J.; Sadar, M. D.; Sin, D. D.; Kuzyk, M.; Xing, L.; Kondra, J.; McWilliams, A.; Man, S. F. P.; Lam, S. Connective

Tissue-Activating Peptide III: A Novel Blood Biomarker for Early Lung Cancer Detection. *J. Clin. Oncol.* **2009**, *27*, 2787–2792.
6. Zhu, W.; Wang, X.; Ma, Y.; Rao, M.; Glimm, J.; Kovach, J. S. Detection of Cancer-Specific Markers Amid Massive Mass Spectral Data. *Proc. Natl. Acad. Sci. U.S.A.* **2003**, *100*, 14666–14671.
7. Wei, F.; Ho, C.-M. Aptamer-Based Electrochemical Biosensor for Botulinum Neurotoxin. *Anal. Bioanal. Chem.* **2009**, *393*, 1943–1948.
8. Chah, S.; Hammond, M. R.; Zare, R. N. Gold Nanoparticles as a Colorimetric Sensor for Protein Conformational Changes. *Chem. Biol.* **2005**, *12*, 323–328.
9. Sandros, M. G.; Gao, D.; Benson, D. E. A Modular Nanoparticle-Based System for Reagentless Small Molecule Biosensing. *J. Am. Chem. Soc.* **2005**, *127*, 12198–12199.
10. Arosio, P.; Ingrassia, R.; Cavadini, P. Ferritins: A Family of Molecules for Iron Storage, Antioxidation and More. *Biochim. Biophys. Acta* **2009**, *1790*, 589–599.
11. Guss, B.; Eliasson, M.; Olsson, A.; Uhlen, M.; Frej, A. K.; Jornvall, H.; Flock, J. I.; Lindberg, M. Structure of the IgG-Binding Regions of Streptococcal Protein G. *EMBO J.* **1986**, *5*, 1567–1575.
12. Paborsky, L. R.; Dunn, K. E.; Gibbs, C. S.; Dougherty, J. P. A Nickel Chelate Microtiter Plate Assay for Six Histidine-Containing Proteins. *Anal. Biochem.* **1996**, *234*, 60–65.
13. Hruban, R. H.; Maitra, A.; Goggins, M. Update on Pancreatic Intraepithelial Neoplasia. *Int. J. Clin. Exp. Pathol.* **2008**, *1*, 306–316.
14. Caskey, J. H.; Jones, C.; Miller, Y. E.; Seligman, P. A. Human Ferritin Gene Is Assigned to Chromosome 19. *Proc. Natl. Acad. Sci. U.S.A.* **1983**, *80*, 482–486.
15. Worwood, M.; Brook, J. D.; Cragg, S. J.; Hellkuhl, B.; Jones, B. M.; Perera, P.; Roberts, S. H.; Shaw, D. J. Assignment of Human Ferritin Genes to Chromosomes 11 and 19q13.3→19qter. *Hum. Genet.* **1985**, *69*, 371–374.
16. Derrick, J. P.; Wigley, D. B. Crystal Structure of a Streptococcal Protein G Domain Bound to an Fab Fragment. *Nature* **1992**, *359*, 752–754.
17. Hainfeld, J. F.; Liu, W.; Halsey, C. M. R.; Freimuth, P.; Powell, R. D. Ni–NTA–Gold Clusters Target His-Tagged Proteins. *J. Struct. Biol.* **1999**, *127*, 185–198.
18. Kato, K.; Lian, L.-Y.; Barsukov, I. L.; Derrick, J. P.; Kim, H.; Tanaka, R.; Yoshino, A.; Shiraishi, M.; Shimada, I.; Arata, Y.; *et al.* Model for the Complex between Protein G and an Antibody Fc Fragment in Solution. *Structure* **1995**, *3*, 79–85.
19. Sauer-Eriksson, A. E.; Kleywegt, G. J.; Uhlén, M.; Jones, T. A. Crystal Structure of the C2 Fragment of Streptococcal Protein G in Complex with the Fc Domain of Human Igg. *Structure* **1995**, *3*, 265–278.
20. Saha, K.; Bender, F.; Gizeli, E. Comparative Study of Igg Binding to Proteins G and A: Nonequilibrium Kinetic and Binding Constant Determination with the Acoustic Waveguide Device. *Anal. Chem.* **2003**, *75*, 835–842.
21. Schmitt, J.; Hess, H.; Stunnenberg, H. Affinity Purification of Histidine-Tagged Proteins. *Mol. Biol. Rep.* **1993**, *18*, 223–230.
22. Medintz, I. L.; Uyeda, H. T.; Goldman, E. R.; Mattoussi, H. Quantum Dot Bioconjugates for Imaging, Labelling and Sensing. *Nat. Mater.* **2005**, *4*, 435–446.
23. Michalet, X.; Pinaud, F. F.; Bentolila, L. A.; Tsay, J. M.; Doose, S.; Li, J. J.; Sundaresan, G.; Wu, A. M.; Gambhir, S. S.; Weiss, S. Quantum Dots for Live Cells, *in Vivo* Imaging, and Diagnostics. *Science* **2005**, *307*, 538–544.
24. Lee, K. H.; Galloway, J. F.; Park, J.; Dvoracek, C. M.; Dallas, M.; Konstantopoulos, K.; Maitra, A.; Searson, P. C. Quantitative Molecular Profiling of Biomarkers for Pancreatic Cancer with Functionalized Quantum Dots. *Nanomedicine* **2012**, *8*, 1043–1051.
25. Park, H.; Lee, J. W.; Hwang, M. P.; Lee, K. H. Quantification of Cardiovascular Disease Biomarkers *via* Functionalized Magnetic Beads and on-Demand Detachable Quantum Dots. *Nanoscale* **2013**, *5*, 8609–8615.
26. Nichols, L. S.; Ashfaq, R.; Iacobuzio-Donahue, C. A. Claudin 4 Protein Expression in Primary and Metastatic Pancreatic Cancer: Support for Use as a Therapeutic Target. *Am. J. Clin. Pathol.* **2004**, *121*, 226–230.
27. Conti, M.; Falini, G.; Samorì, B. How Strong Is the Coordination Bond between a Histidine Tag and Ni–Nitrilotriacetate? An Experiment of Mechanochemistry on Single Molecules. *Angew. Chem., Int. Ed.* **2000**, *39*, 215–218.
28. Park, H.; Hwang, M. P.; Lee, J. W.; Choi, J.; Lee, K. H. Harnessing Immunomagnetic Separation and Quantum Dot-Based Quantification Capacities for the Enumeration of Absolute Levels of Biomarker. *Nanotechnology* **2013**, *24*, 285103.
29. Leatherdale, C. A.; Woo, W. K.; Mikulec, F. V.; Bawendi, M. G. On the Absorption Cross Section of CdSe Nanocrystal Quantum Dots. *J. Phys. Chem. B* **2002**, *106*, 7619–7622.
30. Chevalier, S. B.; Cuestas-Ayllon, C.; Grazu, V.; Luna, M.; Feracci, H.; de la Fuente, J. M. Creating Biomimetic Surfaces through Covalent and Oriented Binding of Proteins. *Langmuir* **2010**, *26*, 14707–14715.
31. Lin, X.; Xie, J.; Zhu, L.; Lee, S.; Niu, G.; Ma, Y.; Kim, K.; Chen, X. Hybrid Ferritin Nanoparticles as Activatable Probes for Tumor Imaging. *Angew. Chem., Int. Ed.* **2011**, *50*, 1569–1572.
32. Lawson, D. M.; Treffry, A.; Artymiuk, P. J.; Harrison, P. M.; Yewdall, S. J.; Luzzago, A.; Cesareni, G.; Levi, S.; Arosio, P. Identification of the Ferroxidase Centre in Ferritin. *FEBS Lett.* **1989**, *254*, 207–210.
33. Torti, F. M.; Torti, S. V. Regulation of Ferritin Genes and Protein. *Blood* **2002**, *99*, 3505–3516.
34. Aime, S.; Frullano, L.; Geninatti Crich, S. Compartmentalization of a Gadolinium Complex in the Apoferritin Cavity: A Route to Obtain High Relaxivity Contrast Agents for Magnetic Resonance Imaging. *Angew. Chem., Int. Ed.* **2002**, *41*, 1017–1019.
35. Fan, K.; Cao, C.; Pan, Y.; Lu, D.; Yang, D.; Feng, J.; Song, L.; Liang, M.; Yan, X. Magnetoferritin Nanoparticles for Targeting and Visualizing Tumour Tissues. *Nat. Nanotechnol.* **2012**, *7*, 459–464.
36. Ma-Ham, A.; Wu, H.; Wang, J.; Kang, X.; Zhang, Y.; Lin, Y. Apoferritin-Based Nanomedicine Platform for Drug Delivery: Equilibrium Binding Study of Daunomycin with DNA. *J. Mater. Chem.* **2011**, *21*, 8700–8708.